IEEE Access
Multidisciplinary | Rapid Review | Open Access Journal

Received February 17, 2018, accepted April 17, 2018, date of publication April 27, 2018, date of current version May 16, 2018.

Digital Object Identifier 10.1109/ACCESS.2018.2830975

Detection and Denoising of Microseismic Events Using Time–Frequency Representation and Tensor Decomposition

NAVEED IQBAL[1], ENTAO LIU[2], JAMES H. MCCLELLAN[2], (Life Fellow, IEEE), ABDULLATIF AL-SHUHAIL[1], SANLINN I. KAKA[1], AND AZZEDINE ZERGUINE[1], (Senior Member, IEEE)

[1]Center of Energy and Geo Processing, King Fahd University of Petroleum & Minerals, Dhahran 31261, Saudi Arabia
[2]Center of Energy and Geo Processing, Georgia Institute of Technology, Atlanta, GA 30332, USA

Corresponding author: Naveed Iqbal (naveediqbal@kfupm.edu.sa)

This work was supported by the Center for Energy and Geo Processing at the King Fahd University of Petroleum & Minerals and Georgia Institute of Technology under Project GTEC1311.

ABSTRACT Reliable detection and recovery of a microseismic event in large volume of passive monitoring data is usually a challenging task due to the low signal-to-noise ratio environment. The accuracy of weak microseismic event identification is a very important step in the analysis and interpretation of microseismic data. This paper introduces an approach for detecting (presence indication) and denoising (accurate recovery) microseismic events using tensor decomposition by considering the time–frequency representation of multiple traces as a 3-D tensor. A tensor is a multiway array having dimension greater than two, and recent signal processing techniques have been developed to manipulate such data by taking advantage of the multidimensional structure. With advances in technology and the availability of cheap memory, it is now possible to store and do mathematical operations, such as higher order singular-value decomposition or tensor decomposition, on multiway data. In active seismic, tensor decomposition has been used for multidimensional reconstruction via higher order interpolation to obtain missing observations. In this paper, we use 3-D tensor decomposition to process passive seismic data. Experiments performed on synthetic and field data sets show promising results achieved by these new methods.

INDEX TERMS Tensor decomposition, higher order singular values decomposition (HOSVD), microseismic, denoising, detection, nuclear norm.

I. INTRODUCTION

Microseismic events induced during hydraulic fracturing, reservoir monitoring, geothermal studies and carbon captured and sequestration studies are characterized by small magnitudes. Furthermore, microseismic data is noisy, especially when geophones are located at the surface due to the interference of surface waves. These noisy events may result in incorrect detection and inaccurate location estimates of weak microseismic events. In this work, we consider a multichannel scenario where each trace resulted from the recordings contains a time-delayed arrival from the microseismic event. Before processing a large volume of microseismic data acquired during long-term monitoring, it is necessary to detect the part of the data that contains microseismic events. This avoids subsequent processing of redundant data and reduces the overall computational requirements. *This detection process is also helpful for the parameter estimation methods in seismic (e.g., [2]–[7]) that rely on the part of the data which is without event (noise-only part). Moreover, it can also be used as a preprocessing step in ambient noise studies (e.g., see [8], [9]).* After initial detection, the next step is to denoise the microseismic data for accurate recovery of event signals that can be be used for localization purpose in the later stage of processing. While this field is still evolving, novel and better methods continue to emerge for detecting and enhancing the signal-to-noise ratio (SNR).

Generally, there exit several denoising or SNR enhancement methods in the literature, which are discussed next. Spectral filtering and band-pass filtering are widely used methods for the attenuation of the noise outside the signal

band. However, these filters do not remove the noise fully without distorting the original signal. The signal often shares some frequency bands with noise and hence, these methods are not effective. Spectral filtering can also results in artifacts that can be confused with the original signal [10]. Therefore, more reliable and efficient denoising methods have been proposed for seismic data. Interferometry is another well-known method, which mainly consists of three steps, cross-correlation, alignment, stacking and convolution [11]–[13]. Another similar technique typically used for this purpose is the matched filter technique, in which a high-SNR event (signal) acts as a template or master event to be used for cross-correlation with the noisy seismic record. Recently, Liu *et al.* [14] modify the basic interferometry method and eliminate the alignment step by proposing an auto-correlation based method instead of cross-correlation. With this approach, ambiguities resulted from the alignment step in cross-correlation based methods are removed. A well-known method for detection of an event is Short-term average/long-term average (STA/LTA) method [15] which is used in earthquake seismology. The method works by finding the ratio of energies in two windows (long and short) and then comparing it with a threshold. The performance of STA/LTA method is justified in a high-SNR scenario. Wiener filtering, which is known for more than four decades, is another famous method for denoising of active seismic data. It requires knowledge of signal or noise statistics which are not readily available in practice. This problem is solved by intuitively finding the noise-only part of the active seismic data [2]–[4], [6]. A similar approach is based on Kalman filtering [7]. Note that distinguishing the signal from the noise is the main challenge in passive microseismic scenario in case of a low SNR environment. A different approach that allows the reconstruction of signals from noisy observation is based on time-frequency peak filtering [16]–[19]. This filtering method encodes the noisy signal as the instantaneous frequency of a frequency modulated analytic signal. The signal is recovered by estimating the peak of the time-frequency distribution of the analytic signal. This approach is sensitive to the noise interferences which detract the energy concentration in time-frequency distribution. Add to this, wavelet transform based methods [5], [20]–[23] are another class that decompose the noisy signal using certain type of a mother wavelet. Here, a threshold is necessary to obtain the enhanced signal. Proper selection of the mother wavelet and the number of decomposition levels are some of the hurdles with this method. The basis function (mother wavelet) does not necessarily match with every real signal. A data driven approach that derives the basis function from the noisy signal is called as empirical mode decomposition [24], [25]. However for this case, the basis function might not be accurate due to the strong noise which affects the denoising results in a low SNR environment. Other less famous techniques proposed in the transform domain are: curvelets [26]–[28], contourlets [29], shearlets [30], seislet [31], [32], dreamlet [33]. The list is really long, however, the focus of this work is on rank-reduction method.

Low-rank/reduced-rank modeling generally refers to a category of methods that solve problems by representing variables of interest as reduced-rank matrices. These methods achieved great success in various fields including bioinformatics, data mining, computer vision, and signal processing. Rank reduction is also a popular approach for denoising. The basic assumption behind these methods is that properly sampled seismic data, in the absence of noise, is low rank. Additive noise increases the rank of the seismic data matrix. Hence, denoising can easily be implemented using rank reduction by methods such as the Singular Value Decomposition (SVD), a well-known tool used for rank reduction which preserves only the significant singular values [34]. Conventionally, SVD operates on 2D matrices.

Recently, rank reduction techniques have been applied on tensors to solve the multidimensional (3D or higher) data problems, e.g., in clustering tasks for estimating the number of clusters, in blind source separation for estimating the number of latent signals and in dimensionality reduction for appropriate dimension estimation [35]–[37]. A tensor is a multidimensional array of numerical values with the order defined by the number of dimensions. Tensors are more natural to represent high dimensional data and to extract useful information from high dimensions data rather than reshaping the data into a 2D matrix, which may lose crucial information on one of the axes [38]–[40].

In order to process multidimensional data, many studies introduced tensor-based mathematical tools, with Tucker model [41] as the most frequently used tensor decomposition model. This model includes methods, such as, generalization of matrix SVD to tensors, i.e., higher-order SVD (HOSVD) [38] and denoising methods, e.g., reduced rank approximation to tensors [42], multidimensional wiener filtering (MWF) [43]–[46] and generic kernel Tucker decomposition [47]. Reduced rank or sub-space based methods require to estimate the rank of a tensor. Unlike matrices, where the solution is obtained by truncating the SVD, the approach of finding the best rank is not straight forward for its multilinear counterpart. Hence, the alternating least-squares (ALS) method is proposed for this purpose, which in tensor domain, known as TUCKALS [38], [48]–[50]. In order to estimate only the dominant singular-vectors for fast computation of the ALS method, Marot *et al.* [51] proposed an algorithm based on the fixed point algorithm to estimate an a priori required number of singular vectors. It is shown in [52] that the fixed point algorithm allows real time response for image enhancement and classification, hence it is necessary for the scenarios where the memory and time requirements are significantly important. There are other rank estimation methods like the minimum description length or Bayesian information criteria which are sensitive to noise [53]. Apart from Tucker, another way to decompose a tensor into its low rank components is through the canonical decomposition (CANDECOMP)/parallel factor analysis (PARAFAC) [54], [55]. The PARAFAC-based denoising methods include the rank-1 tensor approximation, e.g., see [56] and [57]. However, the lack

of an efficient way for estimating the rank of PARAFAC is the major constraint for automatic denoising [58]. Furthermore, PARAFAC type decomposition is computationally challenging and best r-rank approximation may not even exist in some cases [59]. In addition to the above mentioned methods, there exists multidimensional wavelet packet transform (MWPT) based methods which have been applied to 3D hyperspectral images [60], [61]. A survey on MWF and PARAFAC methods is done by Lin and Bourennane [58], where a combination of MWF and MWPT is proposed. Unlike MWF and PARAFAC, this novel combination gives better performance and preserves rare signals in the denoising process. *All of the aforementioned methods are based on the assumption of the priori knowledge of the signal and moreover, they are implicitly developed for signals corrupted by additive white gaussian noise [62].*

Tensors are also well known in the seismic field. For example, they are extensively used for data completion of higher dimension (3D, 4D, and 5D) *active seismic* data (see [63], [64] and references therein). In [63], a novel tensor decomposition known as tensor singular-value decomposition (tSVD) is used. The tSVD is developed by Kilmer and Martin [65] for 3D tensors and later extended by Martin *et al.* [66] to higher order tensors.

Motivated by the promising performance of SVD in our previous work [34], in this paper, we introduce a method for detection and denoising of microseismic data using the so-called SVD-like tensor decomposition. We consider microseismic data as a tensor of order 3. Microseismic data is collected by an array of geophones in a downhole or on the ground surface, which is then formatted as 2D data (time and trace number). Our scenario of passive microseismic data is different from that of active seismic data for two reasons. First, passive microseismic data is much noisier than the active case. Second, active seismic data is already multidimensional (3D or more), since it has multiple source records. However, microseismic data has one source record (2D), which motivates us to transform it to a 3D scenario.

One way to denoise microseismic data is to apply rank reduction using matrix SVD on a 2D data array. However, this might not be a good approach in a very noisy environment, as it is the case in microseimic monitoring. Therefore, we transform 2D microseismic data to 3D data using a time-frequency representation (TFR) of each trace and then obtain the desired denoising results by using SVD-like decomposition on the tensor of order 3 whose three dimensions represent frequency, time, and spatial information. The reason we expect good performance with this approach is that the desired signal will be recovered from a 3D tensor (more information) instead of a 2D matrix (less information). Furthermore, SVDs are applied on various components of a 3D tensor which gives a better denoising result as compared to when applying matrix SVD on the whole 2D microseismic data. Lastly, the tensor analysis fully represents the correlation among the traces in time, space and the frequency domains altogether. Denoising method that uses the transformation of a 1D trace to its 2D time-frequency representation is already available in the literature ([5], [16]–[23]). However, for the first time, inspired by the previous transformation, we take the lead to suggest this 3D technique. We move one step further and take the time-frequency representations of all the traces together (tensor), which makes it a 3D tensor problem.

Many high-resolution TFRs have been developed. Among them are the continuous wavelet transform and the short-time Fourier transform (STFT), which are well-known transforms for recovering the signal contents [67]–[69]. Other transforms are synchrosqueezing transform [70], empirical mode decomposition [24], matching pursuit [71] and basis pursuit [72]–[74], to name a few. Here, we will use the STFT [75]–[77], since it is easy to compute (low computational complexity) and invertible.

In this study, two SVD-like tensor decompositions are used, namely, tSVD [65] and HOSVD [38]. The tSVD is used for denoising since it retains the orientation information and it is useful for time-series applications. However, the HOSVD is found to be a good choice for detection purpose only. The reason is that singular values, in this case, contain the moveout[1] information, which is lost when low-rank approximation is performed by shrinking the singular values.

In summary, the main contributions of this work are:

- Development of a method for detection of passive events using HOSVD.
- Development of a method for denoising of microseismic data using tSVD.
- Development of a method for threshold identification in tSVD.
- Development of a method for denoising/detection in presence of correlated noise.
- Demonstration of the effectiveness of the proposed method using synthetic and field microseismic data sets.
- Demonstration of the performance superiority of the proposed method over other methods.

In [1], we have presented synthetic results for tSVD only and therefore, the work reported here completes the whole study that is not found in [1]. The rest of this paper is organized as follows. Section II is devoted to the mathematical background of tools used in this work together with problem formulation. Detection using the HOSVD and denoising using tSVD are presented in Section III and Section IV, respectively. Denoising/detection in presence of correlated noise is discussed in Section V. In Section VI, theoretical findings are validated using synthetic and real data set. Finally, Section VII draws the conclusions.

II. MATHEMATICAL BACKGROUND AND PROBLEM FORMULATION

In this section, mathematical background about TFR, SVD, and tensors is presented, followed by a precise problem formulation.

[1]Moveout is the difference in arrival times of waves (P and S) at each geophone in an array.

A. SHORT TIME FOURIER TRANSFORM (STFT)

Consider G geophones for collecting microseismic data. Each sensor records a time series of sampled measurements at time instant $t = nT$, say y_n^i, as

$$y_n^i = s_n^i + w_n^i, \quad i = 1, 2, \cdots, G \tag{1}$$

where s_n^i and w_n^i represent the signal and noise, respectively (the procedure is done for all the traces, therefore, we ignore the superscript i for simplicity)

The STFT is computed by applying Fast Fourier Transform (FFT) on subsets of observation (data/trace) points/samples, selected from the trace of M samples (i.e, $\mathbf{y} = [y_0, y_1, \ldots, y_{M-1}]$) using a moving window $\mathbf{w} = [w_0, w_1, \cdots, w_{l-1}]$. The sections are overlapped, so after the FFT is computed for l data points, the window is moved by h data points before calculating the next FFT. Note that, h is the hop size and $l - h$ is the window overlap. Hence, the STFT is defined as,

$$\mathbf{Y}(k, m) = \sum_{p=0}^{l-1} y_{p+mh} w_p \exp\left(\frac{-j2\pi kp}{l}\right),$$
$$k = 0, 1, \cdots, l-1, \quad m = 0, 1, 2, \cdots, \frac{M-l}{h} \tag{2}$$

The time series can be recovered from the STFT as follows: First, the inverse FFT (IFFT) is applied at each time instant

$$\tilde{y}_{p,m} = \frac{1}{l} \sum_{k=0}^{l-1} \mathbf{Y}(k, m) \exp\left(\frac{j2\pi kp}{l}\right),$$
$$p = 0, 1, \cdots, l-1, \ m = 0, 1, 2, \cdots, \frac{M-l}{h} \tag{3}$$

Then, the overlap-add method is used to get the final time-domain data,

$$\mathbf{y} = \frac{h}{\|\mathbf{w}\|_2^2} \sum_{m=0}^{(M-l)/h} \phi(\mathbf{w} \odot \tilde{\mathbf{y}}_m, mh), \tag{4}$$

where $\tilde{\mathbf{y}}_m = [\tilde{y}_{0,m}, \tilde{y}_{1,m}, \cdots, \tilde{y}_{l-1,m}, \underbrace{0, 0, \cdots, 0}_{(M-l) \text{ zeros}}]$, $\phi(\mathbf{a}, b)$ is the circular shift of vector $\mathbf{a}$ by b samples, and $\odot$ is the sample-by-sample multiplication.

B. SVD DECOMPOSITION OF MATRICES

Using the SVD, a 2D matrix $\mathbf{A} \in \mathbb{C}^{P \times Q}$ can be decomposed as

$$\mathbf{A} = \mathbf{U}\mathbf{S}\mathbf{V}^T, \tag{5}$$

where $\mathbf{U} \in \mathbb{C}^{P \times P}$ is a unitary matrix whose columns are the left singular vectors, $\mathbf{V} \in \mathbb{C}^{Q \times Q}$ is a unitary matrix whose columns are the right singular vectors, and $\mathbf{S} \in \mathbb{C}^{P \times Q}$ is the rectangular diagonal matrix of singular values arranged in descending order. The singular values can be extracted as a vector $\mathbf{d} = \text{diag}(\mathbf{S}) = [\sigma_1, \sigma_2, \cdots, \sigma_r]$, where diag is the diagonal operator.

C. PRELIMINARIES ON TENSORS

The SVD is a commonly used tool for analyzing 2D arrays, but it can also be used directly with higher dimensional arrays by extending the concept of SVD with tensor theory. To formally define a tensor, let $\boldsymbol{\mathcal{A}} \in \mathbb{C}^{I_1 \times I_2 \times \cdots \times I_N}$ be an N^{th} order tensor having N indices, where $I_1, I_2, \cdots, I_N$ are the upper limits of each dimension. Thus, a scalar is a zero-order tensor denoted by lowercase italic letters (e.g., a), a vector is a 1st-order tensor denoted by lower case bold letters (e.g., $\mathbf{a}$), a matrix is a 2nd-order tensor denoted by capital bold letters (e.g., $\mathbf{A}$), and arrays with more than two dimensions are higher-order tensors represented by calligraphic letters (e.g., $\boldsymbol{\mathcal{A}}$). The TFR of a set of traces can be represented by a 3rd-order tensor $\boldsymbol{\mathcal{A}} \in \mathbb{C}^{I_1 \times I_2 \times I_3}$, having 3 indices, where I_1, I_2, and I_3 represent total number of frequency samples, time samples, and traces, respectively.

Tensors can be decomposed into slices and fibers (modes) by fixing all indices except for one or two, respectively. A tensor slice is a 2D matrix obtained by fixing one of the three indices in a 3rd-order tensor. For example, a frontal slice of a 3rd order tensor $\boldsymbol{\mathcal{A}}$ is obtained by fixing the 3rd index i_3, denoted as $\mathbf{A}_{::i_3}$. Fixing the 2nd index, we get the lateral (or vertical) slice $\mathbf{A}_{:i_2:}$, and fixing the 1st index, we get the horizontal slice $\mathbf{A}_{i_1::}$. The slices of a 3rd-order tensor are shown in Fig. 1. Each index in a tensor is called a mode, and the upper limit for indices in each mode is the mode dimension. For a 2D matrix, columns and rows are mode-1 and mode-2 fibers, respectively. A 3rd-order tensor has 3 modes (column, row and tube fibers) and the dimension of each mode is I_1, I_2, and I_3 corresponding to the vectors $\mathbf{a}_{:i_2i_3}$, $\mathbf{a}_{i_1:i_3}$, and $\mathbf{a}_{i_1i_2:}$, respectively. For our application, mode-1 (columns) and mode-2 (rows) represent frequency and time, respectively, while mode-3 represents spatial information. For illustration, a 3rd-order tensor containing the TFR of three traces ($G = 3$) is shown in Fig. 2a. The fibers of a 3rd-order tensor are shown in Figs. 2b, 2c, and 2d.

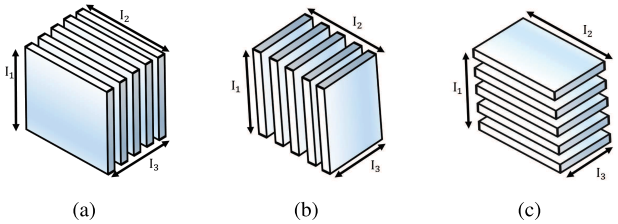

FIGURE 1. Three types of slices for 3rd-order tensor $\boldsymbol{\mathcal{A}} \in \mathbb{C}^{I_1 \times I_2 \times I_3}$. (a) Frontal slices. (b) Lateral slices. (c) Horizontal slices.

D. PROBLEM FORMULATION

The system model in terms of tensor terminology is represented as

$$\boldsymbol{\mathcal{Y}} = \boldsymbol{\mathcal{X}} + \boldsymbol{\mathcal{N}} \tag{6}$$

where $\boldsymbol{\mathcal{X}}$ corresponds to the low-rank component and $\boldsymbol{\mathcal{N}}$ corresponds to the noise component of the tensor $\boldsymbol{\mathcal{Y}}$. The

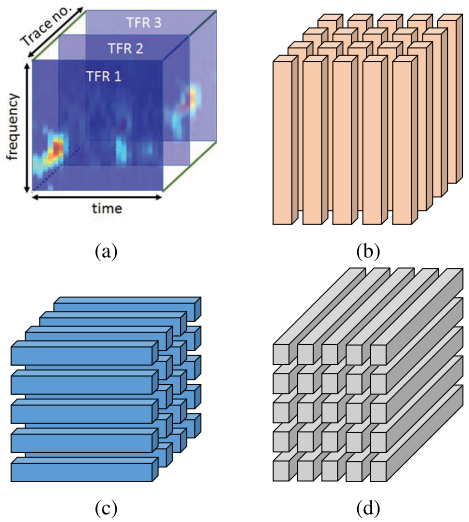

FIGURE 2. Example of 3rd-order tensor and its various Mode-*n* fibers. (a) A 3rd-order tensor. (b) Mode-1 (column) fibers. (c) Mode-2 (row) fibers. (d) Mode-3 (tube) fibers.

frontal slices of $\mathcal{Y}$ are the TFRs corresponding to the time-series traces (as depicted in Fig. 2a). A conventional approach to denoising (via low-rank approximation) is to solve the following optimization problem:

$$\min \text{ rank}(\mathcal{X}) \quad \text{subject to} \quad \|\mathcal{Y} - \mathcal{X}\|_F^2 \leq \delta \tag{7}$$

where $\|\cdot\|_F^2$ is the Frobenius norm which is the sum of the squares of elements of the tensor. This optimization problem (7), which can be interpreted as finding the optimal low-rank estimate of $\mathcal{Y}$ using least-squares, is non-convex and its direct minimization is an NP hard problem [78]. In order to make the minimization tractable, a convex relaxation is employed. The popular choice in this regard is to replace rank($\mathcal{X}$) with the nuclear norm (also called the trace norm) as follows:

$$\min \|\mathcal{X}\|_* \quad \text{subject to} \quad \|\mathcal{Y} - \mathcal{X}\|_F^2 \leq \delta \tag{8}$$

or

$$\min_{\mathcal{X}} J(\mathcal{X}) = \min_{\mathcal{X}} \tfrac{1}{2}\|\mathcal{Y} - \mathcal{X}\|_F^2 + \lambda\|\mathcal{X}\|_* \tag{9}$$

where $\|\cdot\|_*$ is the nuclear norm. For a matrix, the nuclear norm ($\|\cdot\|_*$) is the sum of its singular values, whereas, the nuclear norm of a tensor is the sum of the nuclear norms of the 2nd-order tensors (i.e., matrices) on which the SVD is applied. Candès and Recht [79] demonstrated that low-rank matrices are perfectly recovered by solving the nuclear norm minimization problem. Furthermore, it is shown in [80] that the low-rank approximation of a matrix using nuclear norm minimization together with Frobenius norm fidelity can easily be solved with soft-thresholding of the singular values of the concerned matrix. It is interesting to point out that rank minimization and nuclear norm minimization can be viewed as ℓ_0 and ℓ_1 minimization methods, respectively, in the SVD analysis.

III. DETECTION USING HOSVD

A. HIGHER-ORDER SVD

In the HOSVD, tensors are transformed into 2D matrices as needed for different applications [38]. Rearranging elements of a tensor into a 2D matrix is known as unfolding or matricization. The mode-n unfolding of the tensor $\mathcal{Y}$ is a matrix $\mathbf{Y}_{(n)} \in \mathbb{C}^{I_n \times \prod_{K \neq n} I_K}$ that consists of mode-n fibers stacked into the columns of a matrix. The HOSVD is formed from the SVDs of all the tensor modal unfoldings. For an N^{th} order tensor $\mathcal{Y}$, these SVDs are:

$$\mathbf{U}_K^T \mathbf{Y}_{(K)} = \mathbf{S}_K \mathbf{V}_K^T \quad \text{for } 1 \leq K \leq N, \tag{10}$$

where $\mathbf{U}_K^T$ and $\mathbf{V}_K^T$ are unitary matrices and $\mathbf{S}_K$ contains the singular values of $\mathbf{Y}_{(K)}$ on the diagonal.

The mode-n multiplication of a tensor $\mathcal{Y} \in \mathbb{C}^{I_1 \times I_2 \times \cdots \times I_N}$ with a matrix $\mathbf{U} \in \mathbb{C}^{J_n \times I_n}$ is denoted by $(\mathcal{Y} \times_n \mathbf{U}) \in \mathbb{C}^{I_1 \times I_2 \times \cdots \times I_{n-1} \times J_n \times I_{n+1} \cdots \times I_N}$, where the matrix product $\mathbf{U}\mathbf{Y}_{(n)}$ is the mode-n matricization of the mode-n tensor matrix product. Using the mode-n product operator, $\times_n$, the famous matrix factorization $\mathbf{Y} = \mathbf{U}\mathbf{S}\mathbf{V}^T$ becomes, in tensor framework, $\mathbf{Y} = \mathbf{S} \times_1 \mathbf{U}_1 \times_2 \mathbf{U}_2$. Similarly, the HOSVD decomposes a tensor $\mathcal{Y} \in \mathbb{C}^{I_1 \times I_2 \times \cdots \times I_N}$ into mode products of a core tensor $\mathcal{S} \in \mathbb{C}^{J_1 \times J_2 \times \cdots \times J_N}$ and N mode matrices $\mathbf{U}_n \in \mathbb{C}^{I_n \times J_n}$,

$$\mathcal{Y} = \mathcal{S} \times_1 \mathbf{U}_1 \times_2 \mathbf{U}_2 \times_3 \cdots \times_N \mathbf{U}_N = \mathcal{S} \times_{n=1}^{N} \mathbf{U}_n \tag{11}$$

Fig. 3 provides a pictorial view of (11) for $N = 3$.

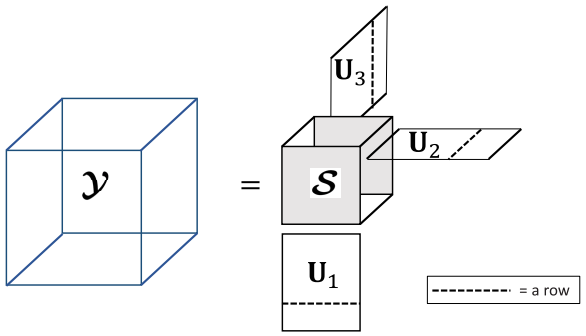

FIGURE 3. Tensor decomposition of third-order tensor $\mathcal{Y} \in \mathbb{C}^{I_1 \times I_2 \times I_3}$ into a core tensor $\mathcal{S} \in \mathbb{C}^{J_1 \times J_2 \times J_3}$ and unitary matrices $\mathbf{U}_1 \in \mathbb{C}^{I_1 \times J_1}, \mathbf{U}_2 \in \mathbb{C}^{I_2 \times J_2}, \mathbf{U}_3 \in \mathbb{C}^{I_3 \times J_3}$.

B. DETECTION OF THE MICROSEISMIC EVENT

For the application of microseismic data denoising, we start by decomposing the 3rd-order tensor into mode-1, mode-2 and mode-3 unfoldings and compute the singular values for each unfolding. The 3 matrix SVDs of the unfoldings that make up the HOSVD are done by taking two independent variables at a time. In other words, taking the SVD of the time-frequency unfolded structure of all the traces, then taking the SVD of the time-space unfolded structure of all the traces, and, third, taking the SVD of the space-frequency unfolded structure of all the traces. The important point to be noted here is that the mode-1 singular values correspond

to the frequency-time contents, mode-2 singular values provide time-space information and mode-3 singular values give space-frequency information.

For detection, we select the largest singular value for all three modes. The reason for selecting only the largest singular value along mode-1, mode-2, and mode-3 is that the maximum energy corresponding to the largest singular value is good enough to detect the event in a whole tensor (TFR of all traces). Thanks to the localized nature of microseismic event in time-frequency domain. The approximation $\hat{\mathcal{X}}_d$ is obtained by discarding the mode-$\mathfrak{n}$ singular vectors corresponding to the mode-$\mathfrak{n}$ singular values except the largest one.

The overall procedure can be cast as follows: first, we find the core tensor as

$$\hat{\mathcal{S}} = \mathcal{Y} \times_1 \bar{\mathbf{U}}_1^H \times_2 \bar{\mathbf{U}}_2^H \times_3 \bar{\mathbf{U}}_3^H, \tag{12}$$

where $(\cdot)^H$ is the Hermitian transpose and $\bar{\mathbf{U}}_\mathfrak{n}$ is the unitary matrix that contains the mode-$\mathfrak{n}$ singular-vector corresponding to the largest mode-$\mathfrak{n}$ singular value, i.e., it contains only the first column of the mode-$\mathfrak{n}$ unitary matrix $\mathbf{U}_\mathfrak{n}$. Second, the detection is carried out as

$$\hat{\mathcal{X}}_d = \hat{\mathcal{S}} \times_1 \bar{\mathbf{U}}_1 \times_2 \bar{\mathbf{U}}_2 \times_3 \bar{\mathbf{U}}_3 \tag{13}$$

Finally, frontal slices of $\hat{\mathcal{X}}_d$ are stacked to get the stacked TFR as

$$\hat{\mathbf{X}}_{sd} = \sum_{i_3} \hat{\mathbf{X}}_{d_{::i_3}} \tag{14}$$

This will enhance the event so that it can be easily be detected in the stacked TFR. The maximum energy in the stacked TFR gives the indication of event presence in microseismic data. Hence, the maximum energy (or the maximum amplitude) is used as a criteria to automatically detect an event in the acquired data set. After detection of an event in a large volume of data, it is now ready for denoising.

IV. DENOISING USING tSVD

A. tSVD

tSVD is based on two operations [65]: t-product, which is a multiplication of two tensors, and t-transpose, which is a transposition operation applied on a tensor. The detailed descriptions of these two operations are as follows:

t-Product: The t-product of two tensors $\mathcal{A}$ of size $I_1 \times I_2 \times I_3$ and $\mathcal{B}$ of size $I_2 \times J \times I_3$ is a tensor $\mathcal{C}$ of size $I_1 \times J \times I_3$, denoted as $\mathcal{C} = \mathcal{A} * \mathcal{B}$. The frontal slices of $\mathcal{C}$ are given as

$$\mathbf{C}_{::i_3} = [\mathbf{A}_{::d_1}, \mathbf{A}_{::d_2}, \cdots, \mathbf{A}_{::d_{I_3}}][\mathbf{B}^T_{::1}, \mathbf{B}^T_{::2}, \cdots, \mathbf{B}^T_{::I_3},]^T, \tag{15}$$

where $d_i = i_3 - i - I_3 \times \lfloor (\frac{i_3 - i}{I_3}) \rfloor + 1$, $\lfloor . \rfloor$ is the floor operator. The t-product uses circulant convolution, as seen in the third index, which can be performed efficiently using the FFT.

t-Transpose: Let $\mathcal{V}$ be a complex-valued tensor of size $I_1 \times I_2 \times I_3$ written in terms of frontal slices as

$$\mathcal{V} = \{\mathbf{V}_{::1}, \mathbf{V}_{::2}, \cdots, \mathbf{V}_{::I_3}\}, \tag{16}$$

then its conjugate transpose $\mathcal{V}^H$ is $I_2 \times I_1 \times I_3$ tensor, which is obtained by conjugate transposing each of the frontal slices and then reversing the order of frontal slices 2 through I_3:

$$\mathcal{V}^H = \{\mathbf{V}^H_{::1}, \mathbf{V}^H_{::I_3}, \mathbf{V}^H_{::I_3-1}, \cdots, \mathbf{V}^H_{::2}\} \tag{17}$$

Using the foregoing definitions, tSVD of a tensor $\mathcal{Y} \in \mathbb{C}^{I_1 \times I_2 \times I_3}$ is defined as

$$\mathcal{Y} = \mathcal{U} * \mathcal{S} * \mathcal{V}^H, \tag{18}$$

where $\mathcal{U}$ and $\mathcal{V}$ are orthogonal $I_1 \times I_1 \times I_3$ and $I_2 \times I_2 \times I_3$ tensor, respectively, and $\mathcal{S}$ is a $I_1 \times I_2 \times I_3$ diagonal tensor which can be calculated as follows: First, FFT is applied on the third dimension of the tensor $\mathcal{Y}$. Next, the SVD of each frontal slice is calculated and finally, the IFFT is applied to the third dimension of the resultant tensors to compute the final tSVD.

B. DENOISING OF THE MICROSEISMIC EVENT

In the denoising operation of microseimic events using tSVD, first the 3rd-order tensor $\acute{\mathcal{Y}}$ is obtained by applying FFT on the third dimension of $\mathcal{Y}$ which can be written in a MATLAB-like syntax as

$$\acute{\mathcal{Y}} = \text{fft}(\mathcal{Y}, [\,], 3) \tag{19}$$

Then, the SVD of the i^{th} frontal slice is computed giving

$$\acute{\mathbf{Y}}_{::i} = \acute{\mathbf{U}}_{::i} \acute{\mathbf{S}}_{::i} \acute{\mathbf{V}}^H_{::i} \qquad \text{for} \quad i = 1, \ldots, I_3 \tag{20}$$

where $\acute{\mathbf{Y}}_{::i}$ is the i^{th} frontal slice of $\acute{\mathcal{Y}}$. Recall the cost function, defined in (9), involves the nuclear norm. In this case, the nuclear norm of a tensor $\mathcal{Y}$ for tSVD is equivalent to the sum of the nuclear norms of all frontal slices of its Fourier transformed version $\acute{\mathcal{Y}}$, i.e.,

$$\|\acute{\mathcal{Y}}\|_* = \sum_{i=1}^{G} \|\acute{\mathbf{Y}}_{::i}\|_* \tag{21}$$

The frontal slices are matrices and the nuclear norm of a matrix $\acute{\mathbf{Y}}$ is defined as $\|\acute{\mathbf{Y}}\|_* = \sum_{j=1}^{\text{rank}(\acute{\mathbf{Y}})} \sigma_j$. Hence, minimizing (9) is equivalent to applying soft thresholding [81] on singular values, i.e., shrinking the singular values of frontal slices, as

$$\mathfrak{s}_j = (\sigma_j - \tau)_+ \tag{22}$$

where τ is the threshold value and $\mathfrak{s}_j$ is the soft thresholding operator on the j^{th} singular value σ_j and $(\cdot)_+ = \max\{0, (\cdot)\}$ extracts the positive part. After applying soft thresholding on $\mathbf{S}_{::i}$, we get

$$\acute{\mathbf{X}}_{::i} = \acute{\mathbf{U}}_{::i} \hat{\acute{\mathbf{S}}}_{::i} \acute{\mathbf{V}}^H_{::i} \tag{23}$$

Along the 3rd dimension, the component tensors are converted back to the time-domain via the IFFT, that is

$$\mathcal{U} = \text{ifft}(\acute{\mathcal{U}}, [\,], 3), \ \mathcal{V} = \text{ifft}(\acute{\mathcal{V}}, [\,], 3), \ \hat{\mathcal{S}} = \text{ifft}(\hat{\acute{\mathcal{S}}}, [\,], 3) \tag{24}$$

and finally, $\hat{\boldsymbol{\mathcal{X}}}$ is given as

$$\hat{\boldsymbol{\mathcal{X}}} = \boldsymbol{\mathcal{U}} * \hat{\boldsymbol{\mathcal{S}}} * \boldsymbol{\mathcal{V}}^H \tag{25}$$

V. DENOISING IN PRESENCE OF CORRELATED NOISE

While performing the experiments, we observe that methods described above give the best performance under white noise (uncorrelated), however, under correlated noise the performance gets affected. Therefore, for correlated noise, the procedure is to whiten the data by removing the minimum-phase part and include it after applying the tensor decomposition method for denoising/detection. This procedure is carried out as follows:

The time samples y_n^i of i^{th} trace is concatenated into a vector of length L as follows:

$$\mathbf{y}_n^i = \left[y_n^i, y_{n-1}^i, , y_{n-2}^i, \cdots y_{n-L}^i\right]^T \tag{26}$$

The minimum-phase part of the observation is obtained from the z-transform of its autocorrelation sequence. In order to estimate the autocorrelation of the observation, and ultimately the z-transform, we first model the observation as an auto-regressive (AR) process. For this purpose, the following model is used for data $\mathbf{y}$ at instant n (again the procedure is done for all the traces, therefore, we ignore the superscript i for simplicity)

$$y_n = -\mathbf{a}_L^T \mathbf{y}_{n-1} + \gamma_n, \tag{27}$$

where $\mathbf{a}_L = [a_1, a_2, \ldots, a_L]^T$ are AR coefficients, $\mathbf{y}_{n-1} = [y_{n-1}, y_{n-2}, \ldots, y_{n-L}]^T$ and γ_n is a white noise process with zero mean and variance σ_γ^2. The Yule-Walker method is used to find $\mathbf{a}_L$. For this, taking the expectation of y_n in (27) after multiplying with $\mathbf{y}_{n-1}^T$, we get

$$E\left\{y_n \mathbf{y}_{n-1}^T\right\} = -E\left\{\mathbf{a}_L^T \mathbf{y}_{n-1} \mathbf{y}_{n-1}^T\right\} + E\left\{\gamma_n \mathbf{y}_{n-1}^T\right\} \tag{28}$$

Under the assumption that the data and noise are uncorrelated, (28) becomes

$$-\mathbf{p}_{yy}^T = \mathbf{a}_L^T \mathbf{P}_{yy} \tag{29}$$

and $\mathbf{a}_L$ is calculated as following:

$$\mathbf{a}_L = -\mathbf{P}_{yy}^{-1} \mathbf{p}_{yy}, \tag{30}$$

where $\mathbf{p}_{yy} = [p_{y,1}, p_{y,2}, \ldots p_{y,L}]^T$, $\mathbf{P}_{yy} =$ Toeplitz $([p_{y,0}, p_{y,1}, \ldots p_{y,L-1}], [p_{y,0}, p_{y,-1}, \ldots p_{y,-L+1}])$, $p_{y,q} = p_{y,-q}$, and $p_{y,q} = \frac{1}{M}\sum_{n=0}^{M-q-1} y_n y_{n+q}$, $q = 0, 1, \ldots, L$. The first column and the first row of the Toeplitz matrix $\mathbf{P}_{yy}$ are $[p_{y,0}, p_{y,1}, \ldots p_{y,L-1}]$ and $[p_{y,0}, p_{y,-1}, \ldots p_{y,-L+1}]$), respectively (here we have used Matlab-like syntax to represent a Toeplitz matrix). A biased form of the estimator is used for $p_{y,q}$ in order to ensure the autocorrelation matrix in (30) is positive semi-definite. This results in a stable AR model. To avoid the matrix inversion in (30), the Levinson-Durbin algorithm [82] is used, which is a recursive and computationally efficient method that exploits the Toeplitz structure of the correlation matrix. Next, (27) can be rewritten as

$$\bar{\mathbf{a}}_L^T \mathbf{y}_n = \gamma_n \tag{31}$$

where $\bar{\mathbf{a}}_L = [1, a_1, a_2, \ldots, a_L]^T$ and $\mathbf{y}_n = [y_n, y_{n-1}, \ldots, y_{n-L}]^T$. Defining a z-domain vector for negative powers as $\mathbf{z}^- = [1, z^{-1}, z^{-2}, \ldots, z^{-L}]^T$, and for positive powers as $\mathbf{z}^+ = [1, z^1, z^2, \ldots, z^L]^T$, the z-transform of (31) looks like the following:

$$Y_n(z)\left(\bar{\mathbf{a}}_L^T \mathbf{z}^-\right) = \gamma(z) \tag{32}$$

Multiplying each side of (32) by its respective time-reversed version gives

$$\Gamma_{yy,n}(z)\left(\bar{\mathbf{a}}_L^T \mathbf{z}^-\right)\left(\bar{\mathbf{a}}_L^T \mathbf{z}^+\right) = \sigma_\gamma^2 \tag{33}$$

Thus, we model the observation by an AR process and the z-transform of the autocorrelation sequence is

$$\Gamma_{yy,n}(z) = \frac{\sigma_\gamma^2}{\underbrace{\left(\bar{\mathbf{a}}_L^T \mathbf{z}^-\right)}_{W(z)}\underbrace{\left(\bar{\mathbf{a}}_L^T \mathbf{z}^+\right)}_{W(z^{-1})}}, \tag{34}$$

where σ_γ^2 can be calculated from (27) as

$$\sigma_\gamma^2 = \frac{1}{M}\sum_{n=L}^{M-1}\left(\bar{\mathbf{a}}_L^T \mathbf{y}_n \mathbf{y}_n^T \bar{\mathbf{a}}_L\right) \tag{35}$$

The data $\mathbf{y}$ is whitened by passing through the whitening filter $1/W(z)$, where $W(z)$ is a minimum-phase polynomial formed from the roots of $\Gamma_{yy,n}(z)$ that fall inside the unit circle in the z-plane. After performing denoising using tensor decomposition, the denoised whitened data is filtered using $W(z)$ to get the final denoised trace. The filter $W(z)$, in the last step, is calculated from the autocorrelation of the ***denoised whitened data*** by first finding $W(z^{-1})$ from the roots of the z-transform of the autocorrelation that fall outside unit circle using a similar procedure as above, and then applying the time-reversal property of the z-transform to get $W(z)$.

VI. EXPERIMENTAL RESULTS

In this section, we validate our theoretical findings using synthetic and field data sets.

A. SYNTHETIC DATA SET WITH WHITE NOISE

For synthetic data, a constant velocity medium is assumed and a Ricker wavelet with dominant frequency of 30 Hz is used. The sampling frequency is set to 500 Hz and forty traces are synthesized with each trace having a duration of 0.4 sec. White Gaussian noise is added to this data set in order to make SNR=−10 dB, consequently, the microseismic event is difficult to detect. The noiseless and noisy synthetic data are shown in Fig. 4a and 4b, respectively (for conciseness, only a portion of the whole data is shown). The STFT processing was carried out with a window length of $l = 100$ and hop size of $h = 2$. To detect this event, (14) is applied to obtain the result shown in Fig. 4c. For a large volume of data, it is recommended to apply the proposed detection method in a sliding window fashion and then the maximum amplitude among all the windows is taken as the presence of an event.

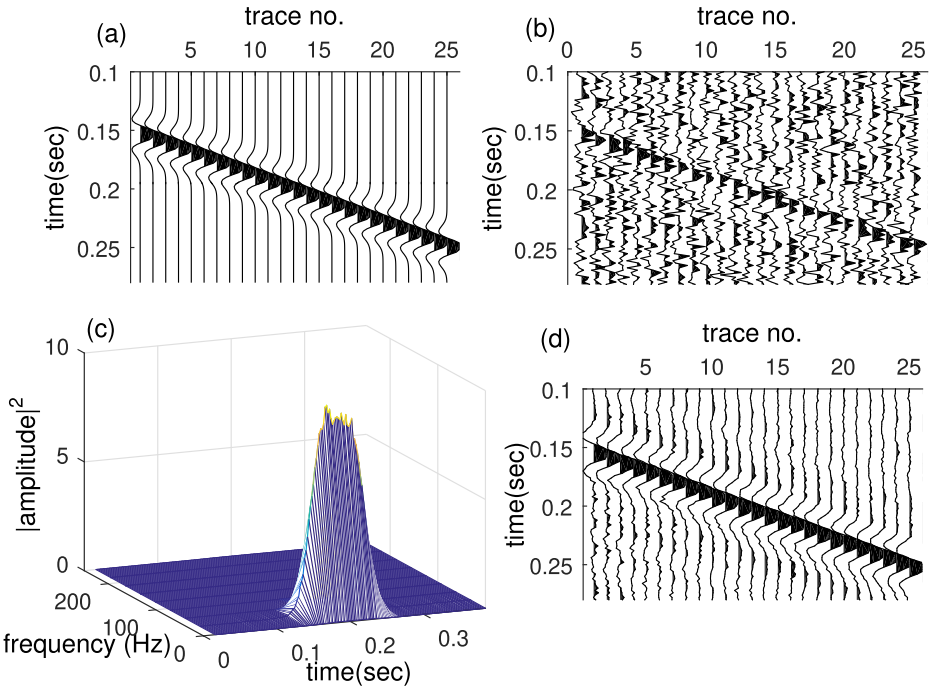

FIGURE 4. Synthetic data test (limited view showing 25 of 40 traces and 0.1 to 0.28 sec): (a) clean data, (b) noisy traces with SNR =−10 dB, (c) detection using HOSVD, $|\hat{\mathcal{X}}_{sd}|^2$, (d) denoised traces using tSVD.

In that case, M will be equal to the length of the sliding window. This will relax the memory requirement needed to store a large 3D array. As can be seen from Fig. 4c, an event of frequency 30 Hz is detected in between 0.1 and 0.25 sec, which is in accordance with Fig. 4a. After initial detection, tSVD is applied for denoising and the near-to-exact matching of denoised traces and noiseless traces can be seen by comparing Figs. 4d and 4a.

An important step in denoising is shrinking the singular values using soft thresholding, which requires a threshold parameter τ. For this purpose, we first plot the singular values of all the frontal slices of $\acute{\mathcal{Y}}$ (see Fig. 5a). From this figure, we conclude that the singular values corresponding to the signal (event) subspace have high values and vice versa. Therefore, to define the threshold τ, singular values obtained for each frontal slice of $\acute{\mathcal{Y}}$ are averaged and then the rate of change of the Averaged Singular Values (ASV) is taken into account. The threshold is defined based on the fact that the rate of change of the singular values belonging to the noise subspace is low. ASV and the rate of change of ASV are shown in Fig. 5b and 5c, respectively. From Fig. 5c, it can be noted that the rate of change is very small for values above -0.2. Therefore, the threshold is defined to lie between the 2nd and 3rd singular value. Hence, from Fig. 5a the value of the threshold τ is set to 292 for synthetic data with white noise. A similar approach of defining the threshold has been proposed for 2D data in signal and image processing fields [83]–[86]. Here, we extend it to the 3D data set. We use this approach instead of the more complex rank estimation methods (mentioned in Section II) because this is a straight

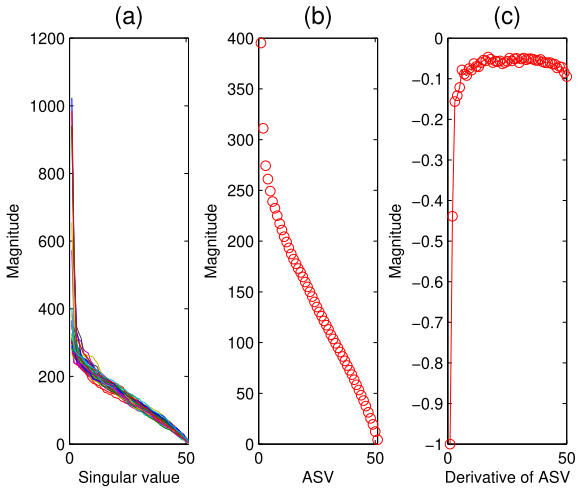

FIGURE 5. (a) Singular values of all frontal slices of $\acute{\mathcal{Y}}$, (b) singular values averaged over all frontal slices (ASV), (c) rate of change of averaged singular values (derivative of ASV) for synthetic data set with white noise.

forward technique without any additional complexity to the denoising method and it is also well-suited to our off line application.

B. SYNTHETIC DATA SET WITH CORRELATED NOISE

Next, same synthetic data set is used with correlated noise (Fig. 6a). SNR is set to the same value as previously. Here, the whitening procedure, as detailed in Section V, is used before denoising. The order of the filter is set to $L = 1$. The reason for selecting the lowest order of the filter is to ensure

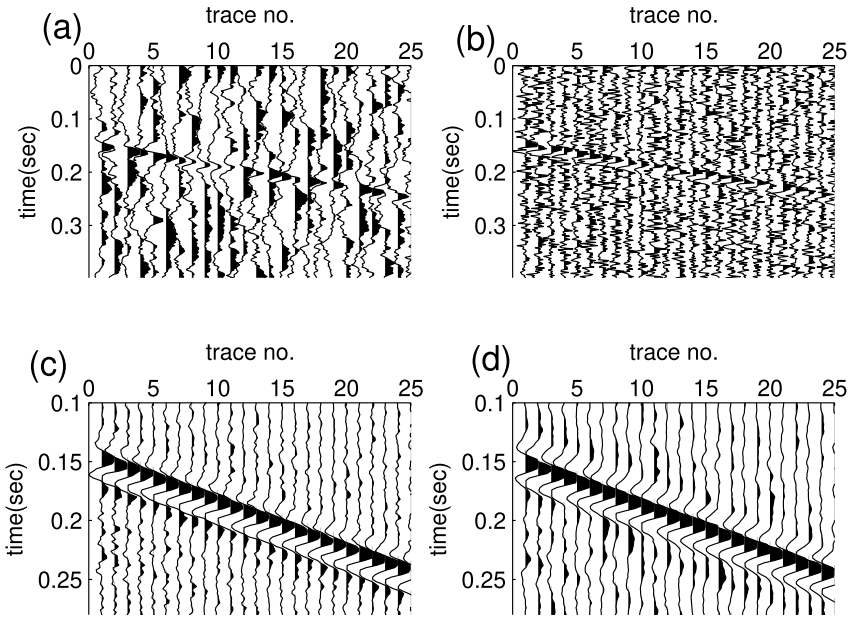

FIGURE 6. Synthetic data in colored noise. (a) Noisy traces with SNR=−10 dB, (b) noisy traces after applying a whitening filter, (c) denoising result (using tSVD) of whitened noisy data, (d) denoised traces after applying inverse whitening filter.

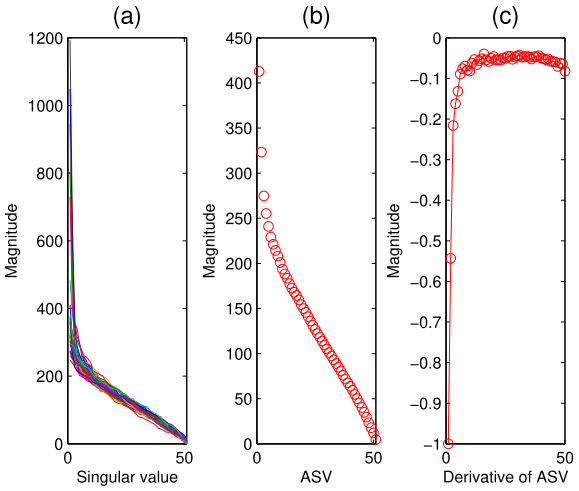

FIGURE 7. (a) Singular values of all frontal slices of $\hat{\mathcal{Y}}$, (b) ASV, (c) rate of change of ASV for synthetic data set with correlated noise.

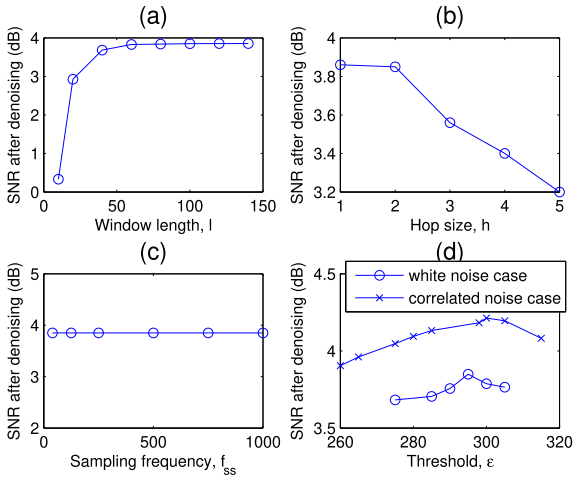

FIGURE 8. Sensitivity analysis of the parameters, (a) window length, l, (b) hope size, h, (c) sampling frequency, f_{ss}, and (d) threshold, ϵ.

that the assumption of no correlation between the noise and microseismic event is still valid. Denoising is performed on whitened noisy data. Ultimately, the final denoised traces are obtained by filtering the denoised whitened data using the inverse whitening filter. The whitened noisy data, denoised whitened data, and the final denoised data are depicted in Figs. 6b, 6c, and 6d, respectively. A similar approach, as in the previous case, is used for defining the threshold; this is shown in Fig. 7. The threshold is defined to lie between the 3rd and 4th singular value. Hence, from Fig. 7a the value of the threshold τ is set to 265 for synthetic data with correlated noise.

C. COMPARISON OF VARIOUS DENOISING METHODS

In order to show the performance superiority of the proposed tensor decomposition based denoising, the proposed technique is compared with the conventional SVD (that is applied on the 2D microseismic data set), wavelet decomposition, empirical mode decomposition, peak filtering, band-pass filtering, and autocorrelation-based denoising methods. Table 1 reports the following metrics used in the comparison: the maximum Correlation Coefficient (CC), Peak-Signal-to-Noise Ratio (PSNR), Signal-to-Noise Ratio (SNR), Mean Absolute Error (MAE), and Mean Square Error (MSE) from the synthetic data experiment (white Gaussian noise case) using the above mentioned denoising methods. For the

TABLE 1. Comparison of the proposed tensor method with other denoising methods.

Method	CC	PSNR	SNR	MAE	MSE	time (sec)
Noisy data set	0.291	5.755	-10.173	2.576	10.36	—
Wavelet decomposition	0.465	11.366	-4.563	0.203	0.073	0.850
Empirical Mode Decomposition	0.457	10.524	-4.731	0.188	0.071	3.470
Bandpass filtering	0.530	11.688	-3.686	0.205	0.068	0.135
Autocorrelation	0.601	12.068	-3.866	0.195	0.062	0.189
Peak filtering	0.494	13.309	-6.464	0.166	0.047	3.528
Conventional SVD	0.451	9.988	-5.941	1.553	3.908	0.980
Proposed tensor method	0.848	19.875	3.850	0.092	0.019	2.120

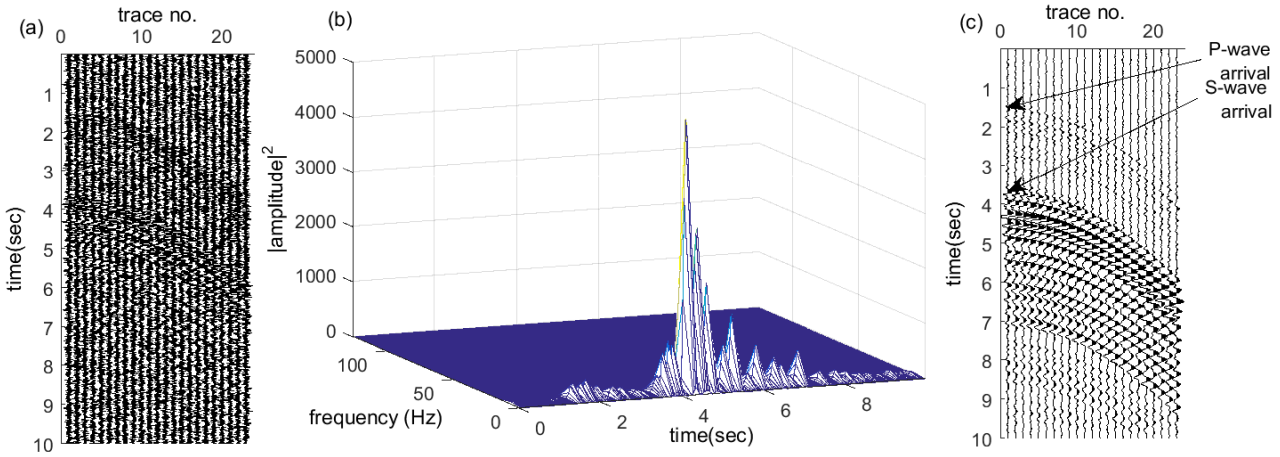

FIGURE 9. (a) Real data set, (b) detection using HOSVD, $|\hat{\mathbf{X}}_{sd}|^2$, (c) denoised traces using tSVD.

wavelet decomposition based denoising technique, we use ''wden'' function in the wavelet toolbox of Matlab [87]. Moreover, we use the principle of Stein's Unbiased Risk for soft thresholding (for details see wavelet toolbox in Matlab2016a and references [5] and [88]). For conventional SVD, empirical mode decomposition, peak filtering and autocorrelation based enhancements methods, we use the methods proposed in [14], [19], [25], and [89], respectively. The reason of the superior performance of our method is justified by the use of the correlation in time and frequency domains together, where as, the other methods either do not use this property at all or use it in only one domain. The complexity of the methods is compared in terms of the running time as shown in Table 1. The time is estimated using an ordinary laptop with core i5 processor running MATLAB 2016a. For the proposed method, we use Matlab toolbox name as ''tensorlab'' [90]. Here, in this study we have propose an application of tensor decomposition in the microseismic field and compare it to the well-known methods to justify the performance of our method. It can be seen from Table 1, except for the computational complexity, our proposed algorithm resulted in the best performance among the rest of the methods.

D. SENSITIVITY ANALYSIS OF THE PARAMETERS

Fig. 8 shows the effect of the window length l, the hope size h, the sampling frequency used for STFT f_{ss} and the threshold ϵ on the SNR enhancement. For the previous synthetic examples we have set the aforementioned parameters based on the experimental analysis. It can be seen from Fig. 8a that as the window size increases, SNR after denoising also increases until a steady state is reached, hence $l = 100$ is a good choice. Conversely, Fig. 8b shows that with increasing the hop size, SNR after denoising decreases, therefore, $h = 2$ (can be set at $h = 1$ with not much SNR enhancement) is used for all the data set used . However, the sampling frequency does not affect the performance as depicted in Fig. 8c. Finally, the effect of the threshold ϵ is shown in Fig. 8d for white and correlated noise. As can be seen from this figure that the maximum SNR is obtained when $\epsilon = 295$. Based on the method presented earlier, the threshold was set to $\epsilon = 292$ for white noise case. Also, as can be seen from this figure, the $\epsilon = 300$ gives the maximum SNR, while the derived value is found to be $\epsilon = 265$ for correlated noise. From this we conclude that the proposed method for the threshold indication is simple and straight forward and, moreover, it is close to the actual threshold (the one that yields maximum SNR enhancement). The SNR enhancement in case of the correlated noise is more as compared with the SNR enhancement in the white noise case, this is due to the fact that in the former case an extra stage of whitening filter is also used.

E. FIELD DATA SET

Finally, the denoising and detection methods are tested on a recorded microseismic trace as depicted in Fig. 9a. The

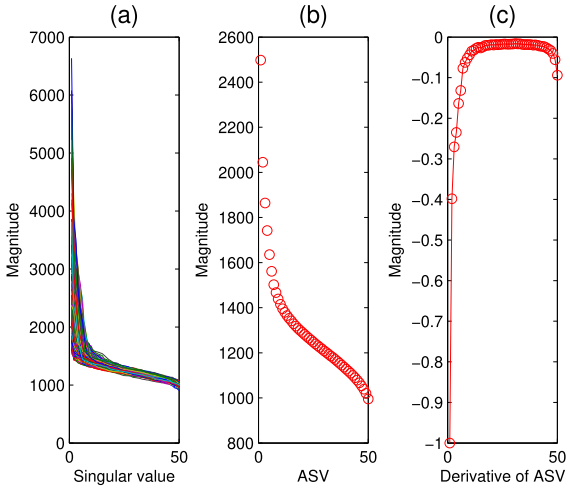

FIGURE 10. (a) Singular values of all frontal slices of $\acute{\mathcal{Y}}$, (b) ASV, (c) rate of change of ASV for field data set.

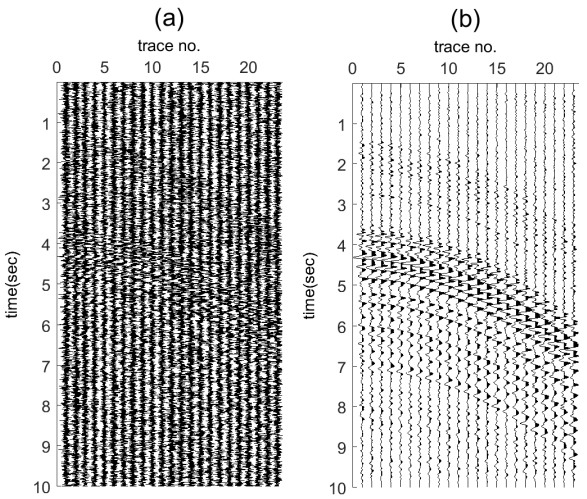

FIGURE 11. (a) Noisy field data set after applying a whitening filter, (b) denoising result of whitened noisy data.

data used in this study is from the High Resolution Seismic Network (HRSN), Berkeley Seismological Laboratory at the University of California, Berkeley (for more details see [14]). The sampling frequency for this data set is 250 Hz. The microseismic event is difficult to detect in this data set, which is apparent from Fig. 9a (showing 23 out of 182 traces). Initially, the detection is carried out using the HOSVD as depicted in Fig. 9b. Detection result shows the presence of an event in between 1 to 7 sec of the data. The denoising result obtained using tSVD is shown in Fig. 9c. It can be seen from the denoised traces that the proposed technique provides an excellent outcome, showing P- and S-wave clearly, for the real field data set. A similar approach, as in the previous cases, is used for defining the threshold as shown in Fig. 10. The threshold is defined to lie between the 4^{th} and 5^{th} singular value. Hence, from Fig. 10a the value of the threshold τ is set to 1688 for field data set. In the case of field data where the nature of the noise is unknown we have passed the data through all the stages of the denoising method, i.e., pre-whitening, denoising and whitening inverse to get the final output. The data after applying the whitening filter and denoising result of the whitened noisy data are shown in Figs. 11a and 11b, respectively. From these figures, it is apparent that the whitening filter has not much effect on the field data set. The reason is that the data has a flat spectrum (white) as depicted in Fig. 12a. Hence, the filter also turns off (see the impulse response of the filter in Fig. 12b). For comparison, we also report the correlated noise case in Fig. 12.

In summary, the proposed method has the following advantages:

- It detects the microseismic event before enhancing it using a simple higher-order SVD technique without defining an explicit complex method for threshold.
- The detection step relaxes the computational requirements by not processing all the data in the denoising step.

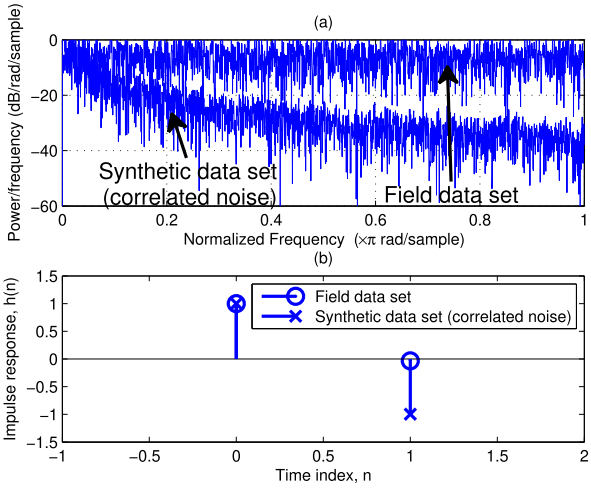

FIGURE 12. (a) Power spectral density estimate of the data, (b) impulse response of the whitening filter.

- Unlike the previously proposed methods, the denoising and detection are performed for the whole 3D tensor and hence, the correlation among the time and frequency contents of the traces are fully utilized.
- In case of denoising, a threshold is defined in a simple and straight forward way.
- The correlated noise case is also embedded.

Finally, note that the threshold is defined in a semi-automatic way.

VII. CONCLUSION

Microseismic data is typically noisy and requires detection and a denoising step before further processing. In this study, reliable multichannel detection and enhancement methods for microseismic events using tensor decomposition are presented. By considering the time-frequency representation of the traces as a third-order tensor, the higher order-singular

value decomposition is used for the aforementioned purposes. The denoised traces are obtained by shrinking the singular values, where a method of obtaining the threshold is also discussed. Tests on synthetic and real seismic data sets show promising detection and denoising results in the presence of uncorrelated and correlated noise.

ACKNOWLEDGMENT

This paper was presented at the 79th European Association of Geoscientists & Engineers (EAGE) Conference and Exhibition, Paris, France, June, 2017 [1].

REFERENCES

[1] N. Iqbal, E. Liu, J. McClellan, A. Al-Shuhail, S. Kaka, and A. Zerguine, "Enhancement of microseismic events using tensor decomposition and time-frequency representation," in *Proc. 79th EAGE Conf. Exhibit.*, Jun. 2017.

[2] J. Wang, F. Tilmann, R. S. White, and P. Bordoni, "Application of frequency-dependent multichannel Wiener filters to detect events in 2D three-component seismometer arrays," *Geophysics*, vol. 74, pp. V133–V141, Nov. 2009.

[3] J. Wang, F. Tilmann, R. S. White, H. Soosalu, and P. Bordoni, "Application of multichannel Wiener filters to the suppression of ambient seismic noise in passive seismic arrays," *Lead. Edge*, vol. 27, pp. 232–238, Feb. 2008.

[4] M. Coughlin *et al.*, "Wiener filtering with a seismic underground array at the sanford underground research facility," *Classical Quantum Gravity*, vol. 31, no. 21, p. 215003, Nov. 2014.

[5] S. M. Mousavi and C. A. Langston, "Hybrid seismic denoising using higher-order statistics and improved wavelet block thresholding," *Bull. Seismological Soc. Amer.*, vol. 106, no. 4, pp. 1380–1393, Aug. 2016.

[6] B. Khadhraoui and A. Özbek, "Multicomponent time-frequency noise attenuation of microseismic data," in *Proc. 75th EAGE Conf. Exhibit. Incorporating (SPE EUROPEC)*, 2013, pp. 200–204.

[7] E. Baziw and I. Weir-Jones, "Application of Kalman filtering techniques for microseismic event detection," *Pure Appl. Geophys.*, vol. 159, pp. 449–471, Jan. 2002.

[8] D. Zigone, Y. Ben-Zion, M. Campillo, and P. Roux, "Seismic tomography of the Southern California plate boundary region from noise-based Rayleigh and love waves," *Pure Appl. Geophys.*, vol. 172, pp. 1007–1032, May 2015.

[9] P. Boué, P. Poli, M. Campillo, H. Pedersen, X. Briand, and P. Roux, "Teleseismic correlations of ambient seismic noise for deep global imaging of the earth," *Geophys. J. Int.*, vol. 194, pp. 844–848, Aug. 2013.

[10] F. Scherbaum, *Of Poles and Zeros: Fundamentals of Digital Seismology*. Dordrecht, The Netherlands: Kluwer, 1996.

[11] I. Mallinson, P. Bharadwaj, G. Schuster, and H. Jakubowicz, "Enhanced refractor imaging by supervirtual interferometry," *Lead. Edge*, vol. 30, no. 5, pp. 546–560, 2011.

[12] A. Al-Shuhail, A. Aldawood, and S. Hanafy, "Application of super-virtual seismic refraction interferometry to enhance first arrivals: A case study from Saudi Arabia," *Lead. Edge*, vol. 31, pp. 34–39, Jan. 2012.

[13] P. Bharadwaj, X. Wang, G. Schuster, and K. McIntosh, "Increasing the number and signal-to-noise ratio of OBS traces with supervirtual refraction interferometry and free-surface multiples," *Geophys. J. Int.*, vol. 192, no. 3, pp. 1070–1084, 2013.

[14] E. Liu *et al.*, "Microseismic events enhancement and detection in sensor arrays using autocorrelation-based filtering," *Geophys. Prospecting*, vol. 65, pp. 1496–1509, Nov. 2017.

[15] J. Wong, L. Han, J. Bancroft, and R. Stewart, "Automatic time-picking of first arrivals on noisy microseismic data," in *Proc. CSEG Conf.*, 2009.

[16] B. Boashash and M. Mesbah, "Signal enhancement by time-frequency peak filtering," *IEEE Trans. Signal Process.*, vol. 52, no. 4, pp. 929–937, Apr. 2004.

[17] X. Deng, H. Ma, Y. Li, and Q. Zeng, "Seismic random noise attenuation based on adaptive time-frequency peak filtering," *J. Appl. Geophys.*, vol. 113, pp. 31–37, Feb. 2015.

[18] C. Zhang, H.-B. Lin, Y. Li, and B.-J. Yang, "Seismic random noise attenuation by time-frequency peak filtering based on joint time-frequency distribution," *Comp. Rendus Geosci.*, vol. 345, pp. 383–391, Sep./Oct. 2013.

[19] P. Yu, Y. Li, H. Lin, and N. Wu, "Seismic random noise removal by delay-compensation time-frequency peak filtering," *J. Geophys. Eng.*, vol. 14, no. 3, pp. 691–697, Jun. 2017.

[20] R. Zhang and T. J. Ulrych, "Physical wavelet frame denoising," *Geophysics*, vol. 68, pp. 225–231, Jan. 2003.

[21] A. C. To, J. R. Moore, and S. D. Glaser, "Wavelet denoising techniques with applications to experimental geophysical data," *Signal Process.*, vol. 89, pp. 144–160, Feb. 2009.

[22] A. Ansari, A. Noorzad, H. Zafarani, and H. Vahidifard, "Correction of highly noisy strong motion records using a modified wavelet de-noising method," *Soil Dyn. Earthquake Eng.*, vol. 30, pp. 1168–1181, Nov. 2010.

[23] M. Beenamol, S. Prabavathy, and J. Mohanalin, "Wavelet based seismic signal de-noising using shannon and tsallis entropy," *Comput. Math. Appl.*, vol. 64, pp. 3580–3593, Dec. 2012.

[24] N. E. Huang *et al.*, "The empirical mode decomposition and the Hilbert spectrum for nonlinear and non-stationary time series analysis," *Proc. Roy. Soc. London Ser. A, Math., Phys. Eng. Sci.*, vol. 454, no. 1971, pp. 903–995, Mar. 1998.

[25] G. Rilling, P. Flandrin, P. Gonçalves, and J. M. Lilly, "Bivariate empirical mode decomposition," *IEEE Signal Process. Lett.*, vol. 14, no. 12, pp. 936–939, Dec. 2007.

[26] F. J. Herrmann and G. Hennenfent, "Non-parametric seismic data recovery with curvelet frames," *Geophys. J. Int.*, vol. 173, pp. 233–248, Apr. 2008.

[27] S. Qu *et al.*, "Deblending of simultaneous-source seismic data using fast iterative shrinkage-thresholding algorithm with firm-thresholding," *Acta Geophys.*, vol. 64, no. 4, pp. 1064–1092, Jan. 2016.

[28] S. Zu *et al.*, "A periodically varying code for improving deblending of simultaneous sources in marine acquisition," *Geophysics*, vol. 81, pp. V213–V225, May 2016.

[29] X. Zhao, Y. Li, G. Zhuang, C. Zhang, and X. Han, "2-D TFPF based on contourlet transform for seismic random noise attenuation," *J. Appl. Geophys.*, vol. 129, pp. 158–166, Jun. 2016.

[30] D. Kong and Z. Peng, "Seismic random noise attenuation using shearlet and total generalized variation," *J. Geophys. Eng.*, vol. 12, no. 6, pp. 1024–1035, Dec. 2015.

[31] Y. Chen, "Iterative deblending with multiple constraints based on shaping regularization," *IEEE Geosci. Remote Sens. Lett.*, vol. 12, no. 11, pp. 2247–2251, Nov. 2015.

[32] Y. Liu, S. Fomel, and C. Liu, "Signal and noise separation in prestack seismic data using velocity-dependent seislet transform," *Geophysics*, vol. 80, pp. WD117–WD128, Nov. 2015.

[33] B. Wang, R.-S. Wu, X. Chen, and J. Li, "Simultaneous seismic data interpolation and denoising with a new adaptive method based on dreamlet transform," *Geophys. J. Int.*, vol. 201, pp. 1182–1194, May 2015.

[34] N. Iqbal, A. Zerguine, S. Kaka, and A. Al-Shuhail, "Automated SVD filtering of time-frequency distribution for enhancing the SNR of microseismic/microquake events," *J. Geophys. Eng.*, vol. 13, no. 6, pp. 964–973, Dec. 2016.

[35] Z. He, A. Cichocki, S. Xie, and K. Choi, "Detecting the number of clusters in n-way probabilistic clustering," *IEEE Trans. Pattern Anal. Mach. Intell.*, vol. 32, no. 11, pp. 2006–2021, Nov. 2010.

[36] A. P. Liavas, P. A. Regalia, and J. P. Delmas, "Blind channel approximation: Effective channel order determination," *IEEE Trans. Signal Process.*, vol. 47, no. 12, pp. 3336–3344, Dec. 1999.

[37] Y. Gao, X. Wang, Y. Cheng, and Z. Wang, "Dimensionality reduction for hyperspectral data based on class-aware tensor neighborhood graph and patch alignment," *IEEE Trans. Neural Netw. Learn. Syst.*, vol. 26, no. 8, pp. 1582–1593, Aug. 2015.

[38] L. De Lathauwer, B. De Moor, and J. Vandewalle, "A multilinear singular value decomposition," *SIAM J. Matrix Anal. Appl.*, vol. 21, no. 4, pp. 1253–1278, 2000.

[39] T. G. Kolda and B. W. Bader, "Tensor decompositions and applications," *SIAM Rev.*, vol. 51, no. 3, pp. 455–500, 2009.

[40] G. Bergqvist and E. Larsson, "The higher-order singular value decomposition: Theory and an application [Lecture Notes]," *IEEE Signal Process. Mag.*, vol. 27, no. 3, pp. 151–154, May 2010.

[41] L. R. Tucker, "Some mathematical notes on three-mode factor analysis," *Psychometrika*, vol. 31, no. 3, pp. 279–311, 1966.

[42] L. De Lathauwer, B. De Moor, and J. Vandewalle, "On the best rank-1 and rank-($R_1, R_2, \ldots, R_N$) approximation of higher-order tensors," *SIAM J. Matrix Anal. Appl.*, vol. 21, no. 4, pp. 1324–1342, 2000.

[43] D. Muti and S. Bourennane, "Survey on tensor signal algebraic filtering," *Signal Process.*, vol. 87, pp. 237–249, Feb. 2007.

[44] D. Letexier and S. Bourennane, "Noise removal from hyperspectral images by multidimensional filtering," *IEEE Trans. Geosci. Remote Sens.*, vol. 46, no. 7, pp. 2061–2069, Jul. 2008.
[45] D. Muti and S. Bourennane, "Multidimensional filtering based on a tensor approach," *Signal Process.*, vol. 85, no. 12, pp. 2338–2353, 2005.
[46] D. Letexier, S. Bourennane, and J. Blanc-Talon, "Nonorthogonal tensor matricization for hyperspectral image filtering," *IEEE Geosci. Remote Sens. Lett.*, vol. 5, no. 1, pp. 3–7, Jan. 2008.
[47] A. Karami, M. Yazdi, and A. Z. Asli, "Noise reduction of hyperspectral images using kernel non-negative tucker decomposition," *IEEE J. Sel. Topics Signal Process.*, vol. 5, no. 3, pp. 487–493, Jun. 2011.
[48] P. M. Kroonenberg and J. de Leeuw, "Principal component analysis of three-mode data by means of alternating least squares algorithms," *Psychometrika*, vol. 45, pp. 69–97, Mar. 1980.
[49] T. Zhang and G. H. Golub, "Rank-one approximation to high order tensors," *SIAM J. Matrix Anal. Appl.*, vol. 23, no. 2, pp. 534–550, Jan. 2001.
[50] E. Kofidis and P. A. Regalia, "On the best rank-1 approximation of higher-order supersymmetric tensors," *SIAM J. Matrix Anal. Appl.*, vol. 23, pp. 863–884, Jan. 2002.
[51] J. Marot, C. Fossati, and S. Bourrennane, "Fast subspace-based tensor data filtering," in *Proc. IEEE Int. Conf. Image Process.*, Nov. 2009, pp. 3869–3872.
[52] B. Cyganek and B. Smołka, "Real-time framework for tensor-based image enhancement for object classification," *Proc. SPIE*, vol. 9897, p. 98970Q, Apr. 2016.
[53] T. Yokota, N. Lee, and A. Cichocki, "Robust multilinear tensor rank estimation using higher order singular value decomposition and information criteria," *IEEE Trans. Signal Process.*, vol. 65, no. 5, pp. 1196–1206, Mar. 2017.
[54] J. D. Carroll and J.-J. Chang, "Analysis of individual differences in multidimensional scaling via an n-way generalization of 'Eckart-Young' decomposition," *Psychometrika*, vol. 35, pp. 283–319, Sep. 1970.
[55] R. Harshman, "Foundations of the parafac procedure: Models and conditions for an 'explanatory' multimodal factor analysis," *UCLA Working Papers Phonetics*, vol. 16, no. 1, pp. 1–84, 1970.
[56] X. Guo, X. Huang, L. Zhang, and L. Zhang, "Hyperspectral image noise reduction based on rank-1 tensor decomposition," *ISPRS J. Photogramm. Remote Sens.*, vol. 83, no. 9, pp. 50–63, Sep. 2013.
[57] X. Liu, S. Bourennane, and C. Fossati, "Denoising of hyperspectral images using the PARAFAC model and statistical performance analysis," *IEEE Trans. Geosci. Remote Sens.*, vol. 50, no. 10, pp. 3717–3724, Oct. 2012.
[58] T. Lin and S. Bourennane, "Survey of hyperspectral image denoising methods based on tensor decompositions," *EURASIP J. Adv. Signal Process.*, vol. 2013, p. 186, Dec. 2013.
[59] V. de Silva and L.-H. Lim, "Tensor rank and the ill-posedness of the best low-rank approximation problem," *SIAM J. Matrix Anal. Appl.*, vol. 30, no. 3, pp. 1084–1127, 2008.
[60] T. Lin and S. Bourennane, "Hyperspectral image processing by jointly filtering wavelet component tensor," *IEEE Trans. Geosci. Remote Sens.*, vol. 51, no. 6, pp. 3529–3541, Jun. 2013.
[61] B. Rasti, J. R. Sveinsson, and M. O. Ulfarsson, "Wavelet-based sparse reduced-rank regression for hyperspectral image restoration," *IEEE Trans. Geosci. Remote Sens.*, vol. 52, no. 10, pp. 6688–6698, Oct. 2014.
[62] C. Li, Y. Ma, J. Huang, X. Mei, and J. Ma, "Hyperspectral image denoising using the robust low-rank tensor recovery," *J. Opt. Soc. Amer. A, Opt. Image Sci.*, vol. 32, p. 1604, Sep. 2015.
[63] G. Ely, S. Aeron, N. Hao, and M. E. Kilmer, "5D and 4D pre-stack seismic data completion using tensor nuclear norm (TNN)," in *Proc. SEG Tech. Program Expanded Abstracts*, Sep. 2013, pp. 3639–3644.
[64] N. Kreimer and M. D. Sacchi, "A tensor higher-order singular value decomposition (HOSVD) for pre-stack simultaneous noise-reduction and interpolation," in *Proc. SEG Tech. Program Expanded Abstracts*, Jan. 2011, pp. 3069–3074.
[65] M. E. Kilmer and C. D. Martin, "Factorization strategies for third-order tensors," *Linear Algebra Appl.*, vol. 435, no. 3, pp. 641–658, 2011.
[66] C. D. Martin, R. Shafer, and B. LaRue, "An order-p tensor factorization with applications in imaging," *SIAM J. Sci. Comput.*, vol. 35, no. 1, pp. A474–A490, Jan. 2013.
[67] M. S. Diallo, M. Kulesh, M. Holschneider, and R. Scherbaum, "Instantaneous polarization attributes in the time–frequency domain and wavefield separation," *Geophys. Prospecting*, vol. 53, no. 5, pp. 723–731, 2005.
[68] M. Kulesh *et al.*, "Polarization analysis in the wavelet domain based on the adaptive covariance method," *Geophys. J. Int.*, vol. 170, no. 2, pp. 667–678, 2007.
[69] A. Roueff, J. Chanussot, J. I. Mars, and M.-Q. Nguyen, "Unsupervised separation of seismic waves using the watershed algorithm on time-scale images," *Geophys. Prospecting*, vol. 52, no. 4, pp. 287–300, 2004.
[70] I. Daubechies, J. Lu, and H. T. Wu, "Synchrosqueezed wavelet transforms: An empirical mode decomposition-like tool," *Appl. Comput. Harmon. Anal.*, vol. 30, no. 2, pp. 243–261, Mar. 2011.
[71] S. G. Mallat and Z. Zhang, "Matching pursuits with time-frequency dictionaries," *IEEE Trans. Signal Process.*, vol. 41, no. 12, pp. 3397–3415, Dec. 1993.
[72] D. Bonar and M. Sacchi, "Complex spectral decomposition via inversion strategies," in *Proc. SEG Annu. Meeting*, 2010, pp. 1408–1412.
[73] I. V. Rodriguez, D. Bonar, and M. Sacchi, "Microseismic data denoising using a 3C group sparsity constrained time-frequency transform," *Geophysics*, vol. 77, pp. V21–V29, Mar. 2012.
[74] R. Zhang and J. Castagna, "Seismic sparse-layer reflectivity inversion using basis pursuit decomposition," *Geophysics*, vol. 76, pp. R147–R158, Nov. s2011.
[75] J. Benesty, M. Sondhi, and Y. Huang, *Springer Handbook of Speech Processing*. Berlin Germany: Springer, 2008.
[76] B. Boashash, *Time-Frequency Signal Analysis and Processing: A Comprehensive Reference*. New York, NY, USA: Elsevier, 2003.
[77] T. Dutoit and F. Marques, *Applied Signal Processing: A MATLAB-Based Proof of Concept*. New York, NY, USA: Springer, 2009.
[78] X. Zhou, C. Yang, H. Zhao, and W. Yu, "Low-rank modeling and its applications in image analysis," *ACM Comput. Surv.*, vol. 47, pp. 1–33, Dec. 2015.
[79] E. J. Candès and B. Recht, "Exact matrix completion via convex optimization," *Found. Comput. Math.*, vol. 9, no. 6, pp. 717–772, 2009.
[80] J.-F. Cai, E. J. Candès, and Z. Shen, "A singular value thresholding algorithm for matrix completion," *SIAM J. Optim.*, vol. 20, no. 4, pp. 1956–1982, 2010.
[81] M. Bachmayr and R. Schneider, "Iterative methods based on soft thresholding of hierarchical tensors," *Found. Comput. Math.*, vol. 17, pp. 1037–1083, Apr. 2016.
[82] S. Haykin, *Adaptive Filter Theory*, 4th ed. Upper-Saddle River, NJ, USA: Prentice-Hall, 2002.
[83] B. K. Natarajan, "Filtering random noise from deterministic signals via data compression," *IEEE Trans. Signal Process.*, vol. 43, no. 11, pp. 2595–2605, Nov. 1995.
[84] K. Konstantinides, B. Natarajan, and G. S. Yovanof, "Noise estimation and filtering using block-based singular value decomposition," *IEEE Trans. Image Process.*, vol. 6, no. 3, pp. 479–483, Mar. 1997.
[85] H. Hassanpour, "A time-frequency approach for noise reduction," *Digit. Signal Process.*, vol. 18, pp. 728–738, Sep. 2008.
[86] X. Lai and M. Zheng, "A denoising method for liDAR full-waveform data," *Math. Problems Eng.*, vol. 2015, pp. 1–8, Jul. 2015.
[87] M. Misiti, Y. Misiti, G. Oppenheim, and J. Poggi, *Wavelet Toolbox for Use With MATLAB*. Natick, MA, USA: The MathWorks, 1996.
[88] C. M. Stein, "Estimation of the mean of a multivariate normal distribution," *Ann. Statist.*, vol. 9, no. 6, pp. 1135–1151, 1981.
[89] J. Wang, X. Meng, L. Guo, Z. Chen, and F. Li, "A correlation-based approach for determining the threshold value of singular value decomposition filtering for potential field data denoising," *J. Geophys. Eng.*, vol. 11, p. 055007, Oct. 2014.
[90] N. Vervliet, O. Debals, L. Sorber, M. Van Barel, and L. De Lathauwer. (Mar. 2016). *Tensorlab 3.0*. [Online]. Available: https://www.tensorlab.net/

NAVEED IQBAL received the B.S. and M.S. degrees in electrical engineering from the University of Engineering and Technology, Peshawar, Pakistan, and the Ph.D. degree from the King Fahd University of Petroleum & Minerals (KFUPM), Saudi Arabia. He was a Post-Doctoral Fellow in electrical engineering at KFUPM from 2014 to 2016. He is currently a Research Engineer with the Center for Energy and Geo Processing, KFUPM. His research interests include adaptive algorithms, compressive sensing, heuristic algorithms, and seismic signal/image processing and acquisition.

ENTAO LIU received the B.S. degree in applied mathematics from Shandong University, Jinan, China in 2005, and the Ph.D. degree in applied mathematics from the University of South Carolina in 2011. He is currently a Post-Doctoral Associate with the Center for Energy and Geo Processing, Georgia Institute of Technology. His research interests include signal processing, seismic imaging, machine learning, numerical analysis, and inverse problems.

JAMES H. McCLELLAN received the B.S. degree in electrical engineering from Louisiana State University, in 1969, and the M.S. and Ph.D. degrees from Rice University in 1972 and 1973, respectively. From 1973 to 1982, he was a member of the research staff at the Lincoln Laboratory and then a Professor at Massachusetts Institute of Technology. From 1982 to 1987, he was with Schlumberger Well Services. Since 1987, he has been a Professor with the School of Electrical and Computer Engineering, Georgia Institute of Technology, where he currently holds the John and Marilu McCarty Chair. In 1987, he received the Technical Achievement Award for work on FIR filter design, and in 1996, the Society Award, both from the IEEE Signal Processing Society. In 2004, he was a co-recipient of the IEEE Jack S. Kilby Signal Processing Medal.

ABDULLATIF AL-SHUHAIL received the B.S. degree in geophysics from the King Fahd University of Petroleum & Minerals (KFUPM) in 1988, and the M.S. and Ph.D. degrees in geophysics from Texas A&M University in 1993 and 1998, respectively. He is an Associate Professor of geophysics with KFUPM. Since then, he has been teaching and advising at KFUPM. He founded and directed the Near Surface Seismic Investigation Consortium at KFUPM from 2006 to 2008. He authored and co-authored several papers in the field of petroleum seismic exploration. He is a co-author of the book *Processing of Seismic Reflection Data Using MATLAB* (Morgan & Claypool Publishers, 2011). His interests include near-surface effects on petroleum seismic data, seismic investigation of fractured reservoirs, and ground penetrating radar. He is an Active Member of the Society of Exploration Geophysicists, the European Association of Geoscientists & Engineers, and the Dhahran Geoscience Society.

SANLINN I. KAKA received the Ph.D. degree in earth sciences from Carleton University, Ottawa, ON, Canada, in 2006. He is currently a Faculty Member and a Graduate Coordinator with the Department of Geosciences, King Fahd University of Petroleum & Minerals. His research interests are in the areas of engineering seismology, reservoir characterization and monitoring, ground-motions relations, and near surface geophysics. His recent research focuses on the applications of microseismic monitoring systems, enhancement, detection, and localization of microseismic events as well as understanding fracture growth and the role of pre-existing fractures during multi-stage hydraulic fracture stimulation of shale gas reservoirs.

AZZEDINE ZERGUINE received the B.Sc. degree from Case Western Reserve University, Cleveland, OH, USA, in 1981, the M.Sc. degree from the King Fahd University of Petroleum & Minerals (KFUPM), Dhahran, Saudi Arabia, in 1990, and the Ph.D. degree from Loughborough University, Loughborough, U.K., in 1996, all in electrical engineering. From 1981 to 1987, he was associated with different Algerian state owned companies. From 1987 to 1990, he was a Research and Teaching Assistant with Electrical Engineering Department, KFUPM, where he is currently a Professor and was involved in signal processing and communications. His current research interests include signal processing for communications, adaptive filtering, neural networks, multiuser detection, and interference cancelation. He was a recipient of three Best Teaching Awards at KFUPM in 2000, 2005, and 2011. He is currently serving as an Associate Editor of the *EURASIP Journal on Advances in Signal Processing*.